

# Quantitative model of volume hologram formation in photopolymers

V. L. Colvin,<sup>a)</sup> R. G. Larson,<sup>b)</sup> A. L. Harris, and M. L. Schilling  
*Bell Laboratories, Lucent Technologies, 700 Mountain Avenue, Murray Hill, New Jersey 07974*

(Received 11 November 1996; accepted for publication 20 January 1997)

A quantitative model is presented to describe the formation of volume holograms in a polymeric medium containing photopolymerizable acrylate monomers that undergo spatially modulated gelation as a result of exposure to a visible “write” beam. The model refines the simple diffusion model of Zhao and Mouroulis [J. Mod. Opt. **41**, 1929 (1994)], by including cure dependence of both the photoreaction kinetics and the monomer diffusivity. These dependences are determined by experimental measurements, using near infrared spectroscopy to quantify the degree of cure and the time dependence of the hologram formation to infer the cure-dependent diffusivity. The cure-dependent diffusion coefficient can be fit by an expression from a free-volume theory, and the cure-dependent reaction rate coefficient is found to be proportional to the diffusivity, showing the reaction rate to be diffusion limited. With the model parameters determined experimentally, predictions are then made of the first, second, and third harmonics of the grating profile, and these are found to be in good agreement with the measured values. The results show the validity of the model and its usefulness in predicting the optimal exposure conditions and performance of a given holographic material. © 1997 American Institute of Physics. [S0021-8979(97)01609-5]

## I. INTRODUCTION

Volume holograms are now under intensive study as possible information storage media because of their potential for achieving storage densities that exceed by more than a decade those readily attainable on laser compact disks. Photopolymers are particularly desirable candidate materials for such holograms because the refractive index changes that can be induced by photoreaction are relatively high,  $\Delta n \sim 10^{-2}$ , compared to the standard inorganic optical material, lithium niobate, for which  $\Delta n \sim 10^{-4}$ , and because photopolymers are more light sensitive than lithium niobate. Photopolymers are also cheap, and can be shaped and processed more readily than inorganic materials.

The hologram writing process in polymers typically involves a photoreaction that occurs preferentially in regions of the sample exposed to high incident radiation fluxes.<sup>1-6</sup> This allows a pattern whose smallest features are of order of the wavelength of light, around  $0.5 \mu\text{m}$ , to be written into the material. If a hologram is to be produced, the chemical reaction must somehow change the index of refraction of the material, and once this change is achieved, it must be stable against degradation that might occur due to continued reactions that occur in the dark, or due to exposure to the hologram read beam. The surest means of stabilizing the hologram is to use up the reactants during the writing process so that none, or almost none, are available for unintended reactions at some later time. But a refractive index gradient must still persist even when all reactants are consumed! This implies that the initially uniform composition or density of the material must be rendered nonuniform during the writing process. This, in turn, implies either that the same reactants

have at least two different nonreversible reactive pathways that they can follow, or that selective diffusive transport must occur over  $w = 0.5 \mu\text{m}$  length scales of the hologram before the reactants are all consumed.

Here we consider only the case where there is a single reaction path, and the refractive index pattern is created by diffusive transport of not-yet reacted species. It is highly desirable that the diffusion time  $t_D$  be of order a minute or less; hence the diffusion coefficient  $D$  should be of order  $w^2/t_D \sim 10^{-10} \text{ cm}^2/\text{s}$ , or so. Fortunately, diffusion coefficients of this order are obtainable in partially cured (or cross linked) polymeric materials, if the temperature of such a material is above its glass transition temperature.<sup>7</sup> Below the glass transition temperature, the polymer becomes too dense and hard to permit diffusion at the needed rate. For optimal recording, the rate of photocuring is also important; as discussed below, it should be comparable to the diffusion rate, or else the material will be under or over exposed, and the holographic pattern will be weak or highly nonlinear.

In the case of a compositional grating, illustrated in Fig. 1, there are two or more components with differing indices of refraction, at least one of which is uncured or only partially cured before hologram writing begins. If the uncured component (monomer) polymerizes, or gels, on exposure to spatially modulated light, a concentration gradient of this monomer will be produced, because of the higher consumption of the monomer in the most intensely illuminated regions of the sample. Diffusion of this monomer will then occur from the dark zones where it is plentiful into light zones where it has been depleted by photoreaction; see Fig. 1. If the other component is already gelled, it will be forced to swell to accommodate the influx of incoming monomer, and a *compositional modulation* will be achieved. Another way to accomplish the same result would be to start with two components that are compatible when in the monomeric state, but phase separate when one of them is polymerized. If the two species react at different rates under exposure to

<sup>a)</sup>Present address: Department of Chemistry, Rice University, Houston, Texas.

<sup>b)</sup>Present address: Department of Chemical Engineering, University of Michigan, Ann Arbor, Michigan 48109. Electronic mail: rlarson@engin.umich.edu

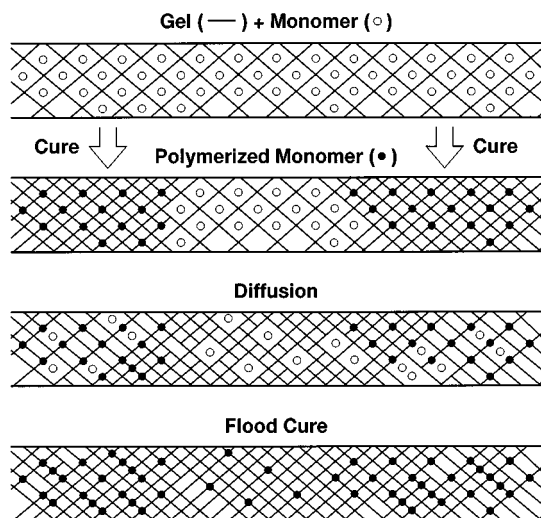


FIG. 1. Illustration of compositional hologram formation in a photopolymer. A polymer gel containing unreacted monomer (○) is exposed to a spatially modulated write beam which cross links the monomer into polymer (●), locking it into the gel in the exposed areas. The remaining unreacted monomer (○) in the relatively unexposed areas then diffuses out of those areas into the exposed areas. A final uniform “flood” exposure locks the remaining monomer into place, leaving a spatial modulation in the concentration of the reacted monomer (●). If the index of refraction of the reacted monomer differs from that of the host gel, the sample will retain a modulation in index of refraction.

light, the less reactive species will selectively migrate out of more polymerized zones.

In either case, once all monomer has reacted and become incorporated into the polymeric gel in a final “flood cure,” a concentration grating will persist, due to the diffusion that had occurred when one or both of the species were still mobile. This concentration grating is illustrated in the bottom drawing of Fig. 1 by a nonuniform concentration of filled circles. The compositional grating manifests itself as a hologram, if the reacted monomer and the original gel matrix have differing indices of refraction.

Photosensitive organic films produced and marketed by the DuPont corporation apparently record compositional holograms by a mechanism similar to that described above.<sup>6,8</sup> This DuPont film consists of a “binder” or thickener, for instance cellulose acetate butyral, containing mobile photoactive monomers, whose exact composition is proprietary.<sup>9</sup> The holographic recording process in this material has been studied experimentally by Zhao and Mouroulis,<sup>8</sup> who compared qualitatively their measurements against the predictions of a diffusion model that they developed<sup>10</sup> for the recording of compositional holograms. The parameters of this model include a diffusion coefficient for the photoactive monomer and a photoreaction kinetic parameter, both of which for the DuPont films are unknown. Zhao and Mouroulis were therefore unable to make direct comparisons between their measurements and the model predictions; nevertheless, their model highlights the important roles played by the relative rates of diffusion and of reaction in the process of hologram formation.

Use of such theoretical models in the design and optimization of materials and recording conditions (such as the pre-

ferred exposure time, exposure intensity, waiting time, etc.), and the design of superior materials for faster writing, greater sensitivity, higher storage density, etc., require *quantitative* testing of the model, using *measured* diffusion and reaction rates. We report here systematic studies of holographic recording in an acrylate-based photopolymer developed by us at Bell Laboratories, along with measurements of kinetic data from which the parameters of the diffusion model can be extracted. An immediate result of the measurements is that both the reaction and diffusion rates are strongly dependent upon cure level. This is expected to be a general result in photopolymer materials, and requires an extension to the simple diffusion model, which we develop and solve numerically. The extended model provides a strikingly good prediction of nonlinear recording effects under the high intensity, extended exposure conditions in our photopolymer. Thus, the essential physical and chemical processes of hologram recording are captured in the extended model.

The rest of the article is organized as follows. In Sec. II, we summarize the Zhao–Mouroulis model and extract salient predictions the model makes for the growth of compositional gratings on exposure to modulated light. Then, in Sec. III, we describe an experimental acrylate photosensitive polymeric system used to test this model, and the methods used to measure the photoreactivities and diffusivities needed as inputs to the model. In Sec. IV, we show the applicability of the model to the acrylate photopolymer system and extract diffusion and reaction rate constants from measurements of reaction kinetics and rates of hologram formation. In Sec. V, we use the model with rate constants determined in Sec. IV to obtain nearly quantitative predictions of the growth of hologram intensity and of the magnitudes of optical nonlinearities when the material is overexposed. The article is summarized in Sec. VI.

## II. REACTION-DIFFUSION MODEL

### A. Summary of the model

The reaction-diffusion model is a one dimensional diffusive transport equation for the concentration  $\phi_m$  of a reacting and diffusing monomer:

$$\frac{\partial}{\partial t} \phi_m = \frac{\partial}{\partial x} \left[ D(\phi_m) \frac{\partial \phi_m}{\partial x} \right] - F(\phi_m) [1 + V \cos(kx)] \phi_m, \quad (1)$$

where the diffusion coefficient  $D(\phi_m)$  depends on the volume fraction  $\phi_m$  of the diffusing monomeric species. The function  $F[1 + V \cos(kx)]$  is the local, time-dependent reaction rate coefficient, which is assumed to be proportional to the local intensity of light, and is therefore a sinusoidal function of position, because the writing beam is created by interference of two laser beams. Here  $k = 2\pi/w$  is the wave-number of the spatial light-intensity pattern, and  $V$  is its visibility, which controls the amplitude of the sinusoidal part of the light intensity relative to the spatially uniform part. For  $V=0$ , the light intensity is uniform, while for  $V=1$ , there are null points where the light intensity drops to zero.

Equation (1) is similar to that used by Zhao and Mouroulis, except that we allow the reaction coefficient  $F(\phi_m)$  to depend on  $\phi_m$ . In addition, we use explicit functions for  $D(\phi_m)$  and  $F(\phi_m)$ , which are matched to experimental diffusion and reaction data, respectively. In applying Eq. (1), we also extend the treatment of Zhao and Mouroulis to consider light pulses of finite duration, which is more typical of exposures used to write multiplexed holograms. Assuming that the refractive index is linear in  $\phi_m$ , one obtains from the concentration profile an index-of-refraction profile that is capable of producing holograms when a read beam is directed through the material.

An important parameter in this model is the *dimensionless reaction rate*,  $F/Dk^2$ . (This parameter is the inverse of the parameter  $R$  defined by Zhao and Mouroulis.<sup>10</sup>) Zhao and Mouroulis found that the intensity of final composition variations, and hence of the final hologram formed, increases with decreasing  $F/Dk^2$ . For *continuous exposure* with  $F/Dk^2 \lesssim 0.1$ , the hologram intensity reaches a limiting value, independent of  $F/Dk^2$ . For large  $F/Dk^2$ ,  $F/Dk^2 \gtrsim 10$ , on the other hand, the photoreaction proceeds too rapidly for diffusion to transport monomer very far before the monomer is entirely consumed by photoreaction. The resulting hologram is therefore weak.

Furthermore, if  $F/Dk^2 > 10$ , the final concentration profile is highly nonsinusoidal; very little of the monomer is able to diffuse a distance equal to  $w/2$ . Thus, the profile consists largely of a small depleted region centered at the point of lowest light intensity. If the concentration profile, and hence index-of-refraction profile, is represented by a Fourier series, one therefore finds that most of the hologram intensity appears in higher harmonics; that is, in harmonics with spatial wavenumbers of  $2k$ ,  $3k$ , etc. Since the read beam typically only reads intensity at the fundamental spatial frequency  $k$ , much of the hologram intensity that is written at high values of  $F/Dk^2$  is wasted. In addition, if multiple holograms are to be superimposed onto each other, then the large nonlinearities inherent in the holograms written at large  $F/Dk^2$  might lead to nonlinear interference among the superimposed holograms, which could limit the number of holograms that can be successfully superimposed. Thus, it would appear that a high diffusion rate, relative to the reaction rate, is the most desirable condition for hologram formation.

Finally, we note that Eq. (1) is one dimensional, implying that there is no variation in polymer or monomer density across the thickness of the sample. Thus, the attenuation of light as it passes through the sample is taken to be small. Furthermore, the rates of polymerization reactions are assumed to respond instantaneously to changes in light intensity; the model neglects the delayed effects of “dark reactions” that are initiated by exposure to light but continue in its absence.

In the following, Sec. II B, we will summarize the predictions of the diffusion model for the case of compositional holograms, for which density changes can be neglected.

## B. Predictions of reaction-diffusion model

To obtain predictions of the model equations for hologram formation in an idealized photoreactive system, we

solve Eq. (1) by a standard central-difference finite difference method, using explicit time integration. The one-dimensional spatial domain is discretized into  $N=20$  intervals of equal length; runs with finer discretizations show that  $N=20$  yields predictions that are precise enough for our purposes. As is well known for explicit integrations, the time step size must be kept small enough to maintain numerical stability.

In this section, the predictions are given in terms of dimensionless quantities; the dimensionless time  $t_D$  and distance  $x_D$  are defined as

$$t_D = tF; \quad x_D \equiv x/w. \quad (2)$$

Since  $F$  is controlled by the intensity of light,  $t_D = tF$  is really a measure of *exposure*. If the exposure were spatially uniform ( $V=0$ ), and the reaction rate were to remain constant with time at its initial rate, then  $t_D=1$  would correspond to the point at which the cure reaches 100%.

The important parameters controlling hologram formation within this model are  $F/Dk^2$ —the ratio of the reaction rate to the diffusion rate, and  $V$ —the fringe visibility. In this section, we gain qualitative insight into the hologram formation process by considering the simplest case, in which  $D=D_0$  and  $F=F_0$  are constants, without a dependence on cure (on  $\phi_m$ ). We consider the  $\phi_m$  dependence in the next section.

To illustrate the mechanism of hologram formation by a diffusion-controlled build-up of a compositional modulation, we consider a case in which  $F_0/D_0k^2=2.5$  and  $V=0.9$ . We shall also assume that the initial composition is 90% polymer gel and 10% unreacted monomer diffusant. The initial polymer gel is assumed to be chemically different from the monomer diffusant, so that even after the diffusant is polymerized, its index of refraction differs (although perhaps only slightly) from that of the original polymer matrix. At all times, we assume volume conservation for simplicity so that the composition of the system is specified by the volume fractions of monomer diffusant,  $\phi_m$ , and polymerized diffusant,  $\phi_p$ . The volume fraction of the initial host matrix polymer is then given by  $\phi_h = 1 - \phi_m - \phi_p$ . The initial composition of the system is here taken to be  $\phi_m=0.1$ ,  $\phi_p=0$ .

Figure 2(a) shows the concentration profile  $\phi_m$  of monomer diffusant at various times, while Fig. 2(b) shows the corresponding concentration profiles of polymerized diffusant  $\phi_p$ . The polymerized diffusant concentration profile initially ( $t_D < 1$ ) develops a sinusoidal spatial variation. With continued exposure, the monomer [Fig. 2(a)] is almost entirely consumed in the high-exposure region, leaving a diminishing monomer “hump” centered on the dark zone. As monomer diffuses out of the dark zone, it reacts to form polymer. For  $F_0/D_0k^2 > 1$  and  $V$  near unity, this reaction occurs faster than diffusion, so that the monomer is polymerized just outside the dark zone to form two small peaks in the final polymer concentration on either side of the deep “trench” in polymer concentration in Fig. 2(b). This profile contrasts with the sinusoidal profile desired from a holographic exposure, and is a result of a finite monomer diffusion rate.

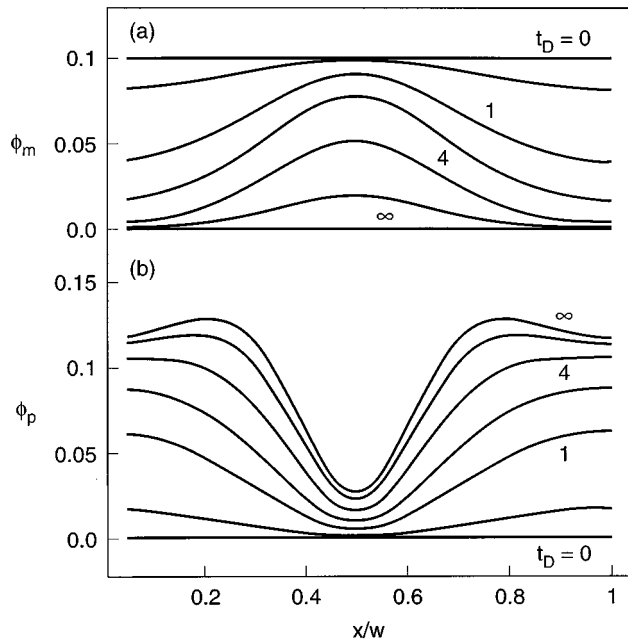


FIG. 2. Profiles of (a) diffusant monomer volume fraction  $\phi_m$ , and (b) diffusant polymer volume fraction  $\phi_p$  at various dimensionless times  $t_D$  after the beginning of writing:  $t_D = Ft = 0, 0.1, 1, 2, 4, 8$ , and  $\infty$ , for  $F_0/D_0k^2 = 2.5$ ;  $V = 0.9$ .

The extent to which the final polymer profile deviates from a sinusoid depends on the ratio  $F_0/D_0k^2$ . For small  $F_0/D_0k^2$ , the monomer diffusion is fast compared to reaction, so the monomer spatial concentration profile remains relatively flat during exposure. Then, the spatial variation in local reaction rate is determined by the sinusoidal light intensity, and the final polymer concentration profile is nearly sinusoidal. Figure 3 shows the final polymer concentration for three values of  $F_0/D_0k^2$ , illustrating the increasingly nonsinusoidal behavior for large  $F_0/D_0k^2$ , at a fixed value of the fringe visibility  $V = 0.9$ . The final polymer profile also depends on  $V$ , which controls the depth of the light intensity null. Figure 4 illustrates the final polymer concentration for several values of  $V$ , at a fixed value of  $F_0/D_0k^2 = 2.5$ . The

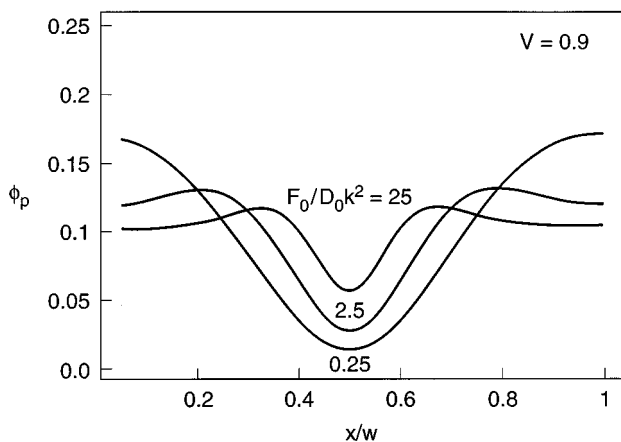


FIG. 3. Profile of polymerized diffusant concentration  $\phi_p$  after writing to complete cure for  $F_0/D_0k^2 = 25, 2.5$ , and  $0.25$ , with  $V = 0.9$ .

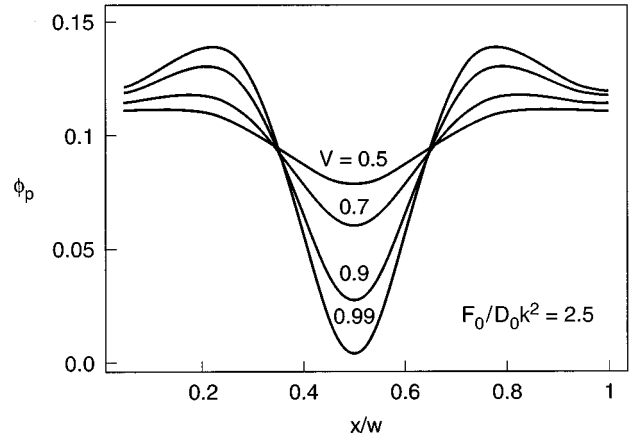


FIG. 4. Profile of polymerized diffusant concentration  $\phi_p$  after writing to complete cure for  $V = 0.5, 0.7, 0.9$ , and  $0.99$ ; with  $F_0/D_0k^2 = 2.5$ .

nonsinusoidal behavior is more pronounced for large values of  $V$ , when the light intensity “null” is strongest.

The magnitudes of the sinusoidal and nonsinusoidal parts of the concentration profiles are quantified in Fig. 5 by the growth of the first and second harmonics of the diffusant concentration profile,  $\Delta\phi_1$  and  $\Delta\phi_2$ . When  $F_0/D_0k^2$  is increased from  $0.25$  to  $2.5$ , the final profile becomes more nonsinusoidal, and the second harmonic increases relative to the first harmonic. A high value of the second harmonic relative to the first harmonic represents a condition of *over exposure*. It is undesirable both because it wastes potential holographic signal, and because when multiple holograms are superimposed onto each other in the same material, it might lead to nonlinear coupling of the superimposed holograms.

Given this behavior, it is of interest to see what happens if the light exposure is turned off before complete cure is reached. Figure 6 shows the build up of the first and second harmonic of the diffusant concentration (in both monomer and polymer forms) with time both when the exposure is continuous, and when it ceases at a dimensionless time  $t_D = t_e F_0 = 1.0$ , where  $t_e$  is the dimensional exposure time.

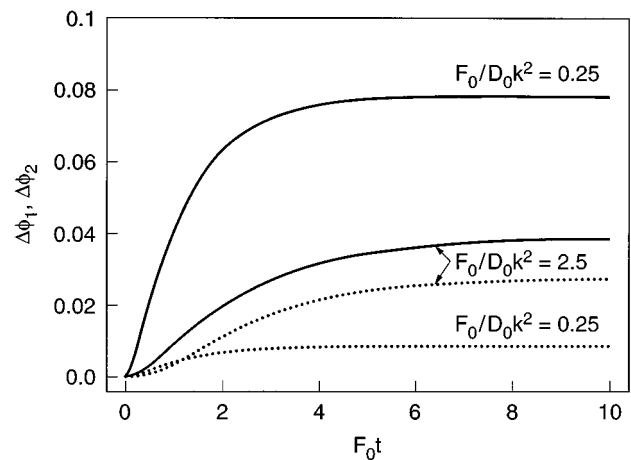


FIG. 5. Time dependence of the first harmonic  $\Delta\phi_1$  (solid line) and second harmonic  $\Delta\phi_2$  (dashed line) of the diffusant concentration profile during hologram writing for  $F_0/D_0k^2 = 0.25$  and  $2.5$  with  $V = 0.9$ .

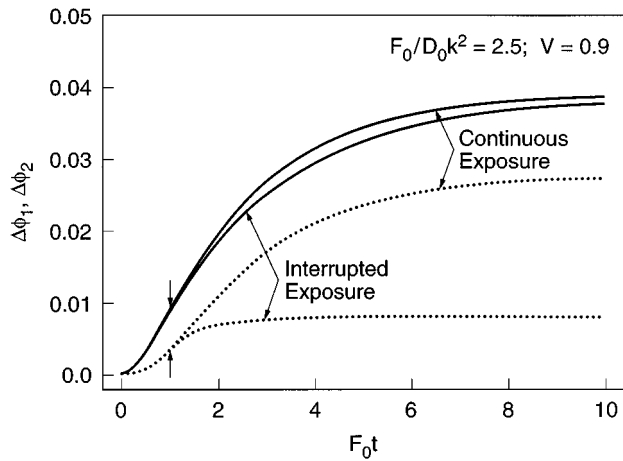


FIG. 6. Time dependence of the first harmonic  $\Delta\phi_1$  (solid lines) and second harmonic  $\Delta\phi_2$  (dashed line) of the diffusant concentration profile during hologram writing for  $V=0.9$ ,  $F_0/D_0k^2=2.5$ , for continuous exposure, and for exposure that is turned off at dimensionless time  $F_0t=1$ , as indicated by the small arrows.

Note that for the interrupted exposure, the first harmonic of the hologram continues to grow even after exposure is halted. This occurs because the monomer gradients produced by the prior exposure continue to drive diffusion even after the light is turned off, leading to continued buildup of holographic intensity. The growth of the second harmonic ceases soon after the exposure ends.

The relative magnitudes of the first and second harmonic grating components are thus strongly dependent upon exposure time, even at high light intensities. This effect proves to be a very useful way to compare experimental data to the model, which we will exploit in Sec. IV. To illustrate the effect that exposure time can have, Fig. 7 shows the first and second harmonics of the final composition pattern (after cessation of diffusion) as functions of dimensionless exposure time  $k^2t_eD_0$ , for various values of dimensionless exposure intensity  $F_0/D_0k^2$ . The “underexposed” condition is distin-

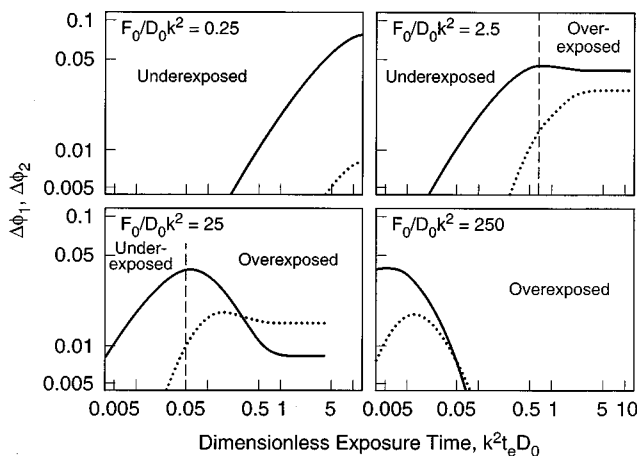


FIG. 7. Final values of the first harmonic  $\Delta\phi_1$  (solid lines) and second harmonic  $\Delta\phi_2$  (dashed line) of the diffusant concentration profile as functions of dimensionless exposure time  $k^2D_0t_e$  for various values of dimensionless exposure intensity  $F_0/D_0k^2$ , with  $V=0.9$ .

guished by a low first harmonic and even lower second harmonic, while in the “overexposed” condition, the second harmonic is nearly as high, if not higher, than the first harmonic. The “optimum” exposure conditions result in large first harmonics and a small ratio of second to first harmonic,  $\Delta\phi_2/\Delta\phi_1 \ll 1$ . Note that optimum exposure conditions can be achieved at any exposure intensity, as long as the exposure time  $t_e$  is adjusted so that  $t_eF_0 \approx 1$ .

While Fig. 7 describes the behavior of an idealized photoreactive material, in real materials the cure-dependent rates of diffusion and reaction complicate the picture. These effects are discussed in Sec. II C.

### C. Cure-dependent reaction and diffusion rates

Reaction-rate measurements to be presented in Sec. IV illustrate a strong concentration dependence of the reaction coefficient for the monomer diffusant in our photopolymer. It is therefore important to include properly the concentration dependence of this coefficient in the hologram reaction-diffusion model. In addition, we will show in Sec. IV that by monitoring the hologram buildup after a short holographic exposure, we can measure the diffusion coefficient of the monomer diffusant in our photopolymer. This diffusion coefficient also shows a strong concentration dependence which must be included in the model. In contrast with these concentration dependencies, we will show that in our photopolymer the dependence on light intensity of the reaction rate is linear, so that the reaction-rate coefficient is nearly constant over a substantial range of intensity values. Were this not so, the sinusoidal spatial dependence in Eq. (1) would need to be modified, and this would be an additional source of nonlinearity in recording. As it is, we need consider only the concentration dependencies, and can assume that the reaction rate coefficient is independent of intensity.

According to the “free volume” theory for polymers that contain a monomeric, plasticizing, species,<sup>11,7,12</sup> the diffusion coefficient should depend on monomer concentration  $\phi_m$  as

$$\left( \ln \frac{D(\phi_m)}{D(0)} \right)^{-1} = K_1 \left( \frac{1}{\phi_m} + K_2 \right), \quad (3)$$

where  $K_1$  and  $K_2$  are constants that can be expressed in terms of the free volume theory as  $K_1 \equiv f_a^2/(\beta B)$ , and  $K_2 \equiv \beta/f_a$ , and  $f_a$ ,  $\beta$ , and  $B$  are parameters of the free-volume theory. In Sec. IV, we show that Eq. (3) provides an adequate description of the diffusion measurements in our photopolymer, with  $K_1$  and  $K_2$  treated as fitting parameters. Thus, Eq. (3) is used to describe  $D(\phi_m)$  in the reaction-diffusion model, using one consistent set of  $K_1$  and  $K_2$  values to model all experiments.

The reaction rate is also found to slow down in more highly cured samples. This slow down, as well as the weak dependence of the reaction coefficient on light intensity mentioned above, is consistent with a reaction rate that is diffusion controlled. If the reaction rate is controlled by the time required for the monomer to diffuse to a reactive site, then the reaction rate coefficient  $F$  should be proportional to the diffusion coefficient. Hence, from Eq. (3), we get

$$F(\phi_m) = IR(0) \exp\left[\frac{1}{K_1(1/\phi_m + K_2)}\right] \propto D(\phi_m), \quad (4)$$

where  $I$  is the exposure intensity of light (in  $\text{mW}/\text{cm}^2$ ), and the coefficient  $R(0)$  is a single fitting parameter, for which we will again choose a “best-fit” value for all experiments.

The extent to which the diffusion and reaction rate vary with concentration of diffusant will obviously differ from one photopolymer to another. We note that without independent measurements of the diffusion and reaction coefficients, modeling of hologram buildup in any photopolymer is necessarily a qualitative exercise only.

### III. MATERIALS AND EXPERIMENTAL METHODS

#### A. Materials

To control photopolymer cure rates and holographic recording properties, a new class of photopolymer was developed, based on photosensitive acrylates. A representative mixture from this class, the *n*-vinyl carbazole “NVC” system, is considered here. It consists of a 10:30:60 (*w/w*)% mixture of *n*-vinyl carbazole, isobornyl acrylate, and polyurethane oligomer. A single step photoinitiator, CG 784S, available from Ciba-Geigy, is added at 1(*w/w*)% to each mixture of acrylate monomers and oligomers. The photoinitiator is a titanocene that absorbs green light efficiently and creates free radicals that then initiate polymerization of acrylate monomeric and oligomeric species.

To create films suitable for recording plane-wave holograms, the viscous acrylate/photoinitiator solutions are held between two glass plates with thicknesses typically around 150–200  $\mu\text{m}$ . With the solution sandwiched in this fashion, oxygen is prevented from inhibiting the acrylate polymerization reaction. The samples are then precured to the desired level by a uniform exposure of 546 nm light using an Oriol model 8436 Hg lamp, with wavelengths less than 530 nm blocked by a filter. At a typical exposure intensity of 10  $\text{mW}/\text{cm}^2$ , the desired precure level (80%–90%) is achieved in approximately 40–70 s. The lamp provides a uniform ( $\pm 5\%$ ) flux of light over a 6 in.  $\times$  6 in. area, allowing several samples to be treated simultaneously. This pre-exposure step both solidifies the viscous acrylate prepolymer and creates a starting cure level optimal for the recording of plane-wave holograms. The precure step thus eliminates the need for a binder, such as that used in the DuPont materials.

The extent of polymerization during precure is measured using near-infrared (NIR) spectroscopy. NIR absorption is an effective method for measurements of reaction kinetics in these acrylate photopolymer samples. The NIR absorption depth in typical polymers is appropriate for 0.1–2.0-mm-thick samples, and the glass substrates are transparent to NIR radiation. The acrylate group has relatively sharp NIR absorptions, appearing at 1620, 2110, and 2220 nm, that are typically distinct from other hydrocarbon absorptions. These absorptions disappear upon polymerization, and are conveniently used to determine the extent of acrylate reaction (double-bond conversion). The NIR spectroscopy does not easily distinguish double-bond conversion of the acrylate groups from that of other terminal double bonds, such as

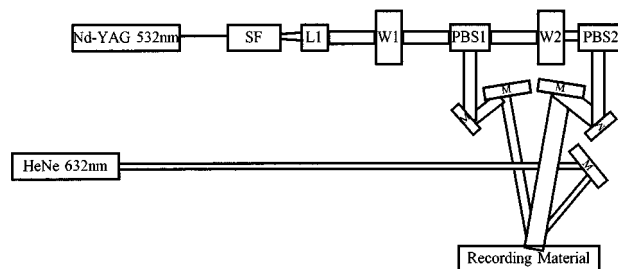


FIG. 8. Light from a diode-pumped Nd-YAG laser (532 nm) is spatially filtered (SF) and collimated (L1) to give a plane-wave beam approximately 1.5 cm in diameter. A polarizing beam splitter (PBS1) produces two beams in the signal and reference arm of the interferometer; each arm has approximately the same length of 225 cm. Two  $\lambda/2$  wave plates (W1 and W2) allow the power of each beam to be varied independently, while ensuring that the final writing beams have only vertical polarization. Interferometric stability is achieved by floating the table, using enclosures over the beam paths, and continually monitoring the laser’s performance in a separate test interferometer. To insure adequate beam overlap, the reference beam is intentionally apertured down to a 7 mm spot, while the signal arm is only apertured to 11 mm in diameter. The two write beams have a  $1/2$  angle of  $18.8^\circ$ ; the HeNe probe beam is brought in at approximately  $3.8^\circ$  higher angle than the reference beam in order to Bragg match it to the hologram.

found in *n*-vinyl carbazole, which is also present and reacting in this material. However, midinfrared kinetics measurements have shown that the conversion of *N*-vinyl carbazole and acrylates in this material are essentially identical throughout the cure process, so that we take the integrated NIR peaks, which include both species, as a measure of cure.

After precure and NIR analysis, samples are wrapped in foil to prevent further light-induced cure, and are stable for at least several weeks. In some cases, no significant change in their recording properties were observed even after several months of storage.

#### B. Recording of holograms

Plane-wave-grating holograms are written into the photopolymer samples by interfering two collimated plane-wave writing beams, the “signal” and “reference” beams, each at 532 nm wavelength. The interference of these two beams produces the sinusoidal spatial intensity to generate a fringe pattern of reaction rate within the sample. The holographic recording setup is shown in Fig. 8. The reference and signal beams have equal (and opposite) angles of incidence on the sample, generating a fringe pattern which is perpendicular to the sample surface (unslanted fringes). The resulting plane-wave holograms are monitored either by diffraction of a probe HeNe laser at 632.8 nm wavelength for real-time monitoring without perturbing the sample cure, or by the readout reference beam at 532 nm wavelength with the signal beam blocked, for the most accurate final-state diffraction measurements.

A diode-pumped, frequency-doubled Nd:YAG laser (Coherent model DPSS-532-400) provides 532 nm recording and readout beams. The laser beam is spatially filtered, expanded to 2 cm diameter, and controllably attenuated to form nearly equal reference and signal beams with intensities,  $I_R$  and  $I_S$ , respectively, ranging from 0.5 to 100  $\text{mW}/\text{cm}^2$ . The

fringe visibility,  $V = 2(I_R I_S)^{1/2}/(I_R + I_S)$  is held near 0.9 for most experiments.

The external incidence angle for recording,  $\theta_E$ , is also the half-angle between the beams. The internal incidence angle within the photopolymer,  $\theta_i$ , is obtained from Snell's law,  $\sin(\theta_i)/n = \sin(\theta_E)/1.0$ , where  $n$  is the index of the photopolymer, with a value close to 1.50 in these experiments. The fringe spacing within the polymer,  $d$ , is then

$$d = \frac{\lambda}{2n \sin(\theta_i)}. \quad (5)$$

The external angle can be varied between 3 and 45 deg, giving grating fringe spacings  $d$  ranging from 5.0 down to 0.37  $\mu\text{m}$ .

A 1 mW HeNe laser (632 nm) provides a probe beam used to monitor the grating formation in real time during or after a recording exposure, without inducing further photoreactions in the sample. This laser is aligned to monitor the first-order grating buildup, at an external angle approximately given by  $\arcsin[(632.8/532.0)\sin(\theta_E)]$ . (This neglects index-of-refraction differences between the red and green wavelengths; experimentally the HeNe diffraction signal is optimized.)

Experiments are carried out in the NVC system using the HeNe probe to explore cure-dependent diffusion. For each experiment, a given level of precure  $\phi_h = 1 - \phi_{m,0}$  is established by the precure lamp and confirmed by NIR spectroscopy, with  $\phi_h$  ranging from 0.86 to 0.96 (monomer concentration 0.14 to 0.04). Weak holographic gratings are written with a 10 s holographic exposure at around 3 mW/cm<sup>2</sup> intensity, typically at a grating period  $d$  of 840 nm, and the diffraction efficiency is measured as a function of time following the exposure, using the HeNe probe. The grating efficiency buildup is interpreted as primarily a diffusive process, and it therefore provides a rough measure of the diffusion constant. The exposures are kept small to minimize the change in cure during the experiment, and the cure level is rechecked after the experiment by NIR spectroscopy. The cure-dependent diffusion constants obtained by this method are presented in Sec. IV.

Once holographic recording is complete, careful measurements of the diffraction efficiencies at various grating orders are made. First, the sample is flood cured to render the sample completely clear and to stabilize the material against further photoinduced reaction. Typically, the flood cure is carried out with a filtered broadband xenon lamp whose light is transmitted to the sample through an optical lightguide. The peak grating efficiency is then obtained by doing an angle scan using a rotation stage at 0.002 deg resolution (Klinger CC1.1), around each Bragg angle to monitor diffraction efficiency from the reference beam onto a large area silicon detector (Newport 818-SL). These angle scans typically show very good agreement with the expected sine-squared shape predicted by coupled-wave theory,<sup>13</sup> and the diffraction efficiency is taken as the central peak-maximum diffraction value. This Bragg peak for the order- $i$  grating occurs at an external angle  $\theta_i$ :

$$\theta_i = \arcsin[i \sin(\theta_E)]. \quad (6)$$

The final peak diffraction efficiency  $E$  obtained from the angle scans provides the refractive index variation for the order- $i$  grating,  $\Delta n_i$ , according to the standard expression valid for unslanted gratings,

$$E = \left[ \sin\left(\frac{\pi \Delta n_i h}{\lambda \cos \theta_{ii}}\right) \right]^2, \quad (7)$$

where  $h$  is the sample thickness and  $\theta_{ii}$  is the internal angle for the order- $i$  read beam. Corrections are also made for reflection losses, which can be substantial for the higher order gratings.

### C. Measurement of cure kinetics

The reaction kinetics, measured as the rate of disappearance of acrylate functional groups, are measured using a single uniform collimated 532 nm beam, with acrylate conversion measured by NIR spectroscopy. Masked samples are used to ensure that the region measured by the NIR spectroscopy is within the uniform beam area. The incident intensity is varied between 1.3 and 93 mW/cm<sup>2</sup>.

To measure the photosensitivity of the NVC system, an 80% precured ( $\phi_{m,0} \approx 0.20$ ) NVC system was prepared and exposed to uniform illumination at a series of intensities. At each intensity, the reaction kinetics were measured in an interrupted cure history making a series of small doses on one sample and measuring the acrylate concentration after each dose. This ensures that the sample temperature does not rise more than a few degrees due to exothermic reactions, so that the reaction kinetics are measured approximately isothermally at room temperature. When strong holograms are written into the sample, temporary temperature rises of up to 10 °C can occur and may affect the details of the kinetics since the cured photopolymer has a broad glass transition temperature at around 35 °C. This effect, which occurs to a much greater extent in actual hologram writing than in the small-dose kinetics measurements, may account for some deviations from predictions of the model. After each dose, NIR measurements were delayed about 3 min to ensure that dark reactions, which are sometimes observed to go on for up to 90 s, were completely extinguished before the acrylate conversion was determined. The same set of experiments was repeated for several different exposure intensities, namely 1.3, 6.0, 7.8, 40, 72, and 93 mW/cm<sup>2</sup>.

To test for the effect of exposure history on reaction kinetics, several samples with the same initial degree of cure  $\phi_m \approx 0.20$ , were each exposed continuously to uniform illumination for differing time durations. The resulting degree of cure was measured for each sample and compared to the degree of cure obtained for samples exposed to an interrupted cure history with the same cumulative exposure dose. As discussed in Sec. IV, a similar degree of cure was obtained in both exposure histories.

## IV. DIFFUSION AND REACTION RESULTS

### A. Cure-dependent diffusivity

The results of several real-time experiments to follow grating buildup after small holographic exposures in samples at varying cure levels are shown in Fig. 9. The grating

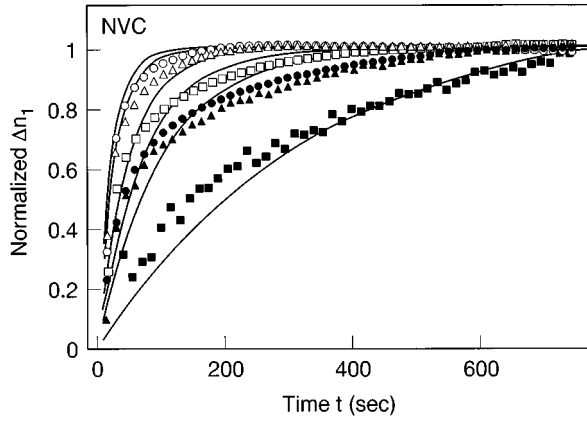


FIG. 9. Growth of normalized index-of-refraction variation  $\Delta n_1$  vs time after short, 10 s cures at exposures of  $3.16 \text{ mW/cm}^2$  with  $d$  spacing of 840 nm, corresponding to an external angle of  $18.3^\circ$ , for samples with initial monomer concentration levels given in Table I. The symbols are data for NVC and the lines are the fits to Eq. (9) with time constants given in Table I. The curves that rise more quickly toward steady state correspond to lower levels of precure.

buildup time is strongly dependent upon cure level, with the most cured samples taking significantly longer to reach full diffraction efficiency. We extract approximate cure-dependent diffusion constants from the data in Fig. 9, under several assumptions. First, we assume that the writing time is fast compared to the diffusion time needed to produce the composition grating, so that most of the grating buildup occurs after writing ceases. Since the writing time in these experiments is only 10 s, this assumption is reasonably accurate. Second, we assume that the local index of refraction is related to that of its constituents by a linear mixing rule. Thus, the index is related to the local concentration of diffusant  $\phi = \phi_m + \phi_p$  by

$$n = (1 - \phi)n^h + \phi n^d = n^h + \phi \Delta n \quad (8)$$

with  $\Delta n \equiv n^d - n^h$  determining the amplitude of the spatial modulations that define the holographic pattern.  $n^h$  and  $n^d$  are the indices of refraction of the host matrix and the diffusant, respectively. Finally, we assume that the exposure is small enough so that the diffusion coefficient  $D$  can be regarded as spatially constant: the sinusoidal composition variation will then grow exponentially. Thus, the index grating, linearly related to the composition grating, will grow as

$$\Delta n_1 \propto 1 - \exp[-\lambda t], \quad (9)$$

where  $\lambda \equiv k^2 D$  is the time constant of the growth.

Figure 9 shows several exponential buildup curves (solid lines), matched to the experimental data. The experimental buildup curves are not particularly well fit by exponentials, and thus the exponential time constants are only a rough approximation of the diffusion process. The nonexponential character of the buildup might arise from partial failure of one or more of the three assumptions underlying Eq. (9). The time constants extracted from these fits do, however, capture the strong cure dependence of the diffusion, and provide a valuable semiquantitative framework for understanding the cure dependence of the reaction kinetics and of the holographic writing process itself under strong hologram condi-

TABLE I. Growth of  $\Delta n_1$  in NVC at  $3.16 \text{ mW/cm}^2$ .

$\phi_{m,0}$	$\phi_{m,f}$	$\bar{\phi}_m \equiv 1/2(\phi_{m,0} + \phi_{m,f})$	Time constant $\lambda \equiv k^2 D \text{ (s}^{-1}\text{)}$
0.142	0.132	0.137	0.044
0.129	0.111	0.120	0.036
0.096	0.089	0.092	0.020
0.089	0.077	0.083	0.014
0.076	0.075	0.075	0.010
0.041	0.039	0.040	0.003

tions (Sec. V). Table I presents the initial monomer concentration  $\phi_{m,0}$ , final monomer concentration  $\phi_{m,f}$ , and exponential time constant  $\lambda$  for the set of samples examined in Fig. 9. The cure level changes are small enough ( $\phi_{m,0} - \phi_{m,f} \approx 0.01$ ) so that each measurement is described by a diffusion constant at roughly a single cure level.

Figure 10 illustrates the cure dependence of the derived diffusion constants from Table I, plotted as  $[\ln(D(\bar{\phi}_m)/D(0))]^{-1}$  vs  $1/\bar{\phi}_m$ , a form which yields the constants  $K_1$  and  $K_2$  of the ‘‘free-volume’’ model [slope  $K_2$  and intercept  $K_1$  of Eq. (3)]. The abscissa in Fig. 10 is  $1/\bar{\phi}_m$ , where  $\bar{\phi}_m$  is the average of the pre and postexposure cures in the Table I. A value of  $\lambda(0)$  at zero monomer concentration is taken to be  $2 \times 10^{-4} \text{ s}^{-1}$ . The data yield a reasonable fit to a straight line, giving some support to the use of the free-volume model for diffusion. The best-fit slope and intercept are  $K_2 = 10.5$  and  $K_1 = 0.0105$ , respectively. When one accounts for the monomer concentration changes that take place during the writing process (see Table I), the growth curves are changed slightly from those predicted from Eq. (9) with the  $\lambda(\bar{\phi}_m)$  values in Table I. When these changes are accounted for by numerically solving Eq. (1) (including also the cure-dependent reaction rate described below), we find that better agreement with the experimental curves can be obtained by using somewhat different values for the constants, namely,  $K_2 = 6.7$  and  $K_1 = 0.0115$ .  $D(0)$  in Eq. (3) is given by  $k^{-2}\lambda(0) = 3.57 \times 10^{-14} \text{ cm}^2/\text{s}$ , and  $k$  for the gratings whose growth is shown in Fig. 9 is  $2\pi/(0.84)^2 \mu\text{m}^{-2}$ .

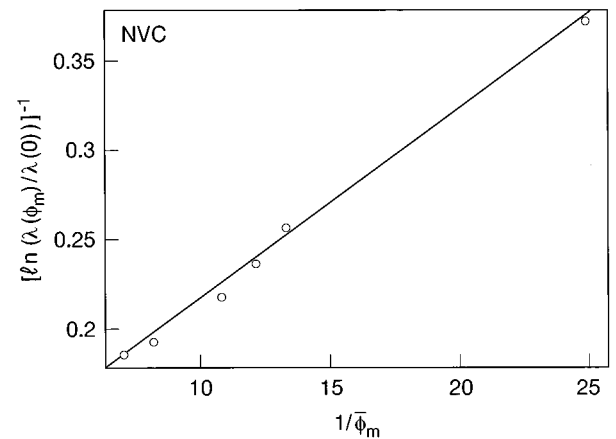


FIG. 10. Plot of  $\{\ln[\lambda(\phi_m)]/\lambda(0)\}^{-1}$  against  $1/\bar{\phi}_m$ , where  $\lambda$  and  $\bar{\phi}_m$  are given in Table I. The value  $\lambda(0)$  at zero monomer concentration was taken to be  $2 \times 10^{-4} \text{ s}^{-1}$ . The line is a fit to the data of Eq. (3), with  $K_1 = 0.0105$  and  $K_2 = 10.5$ .

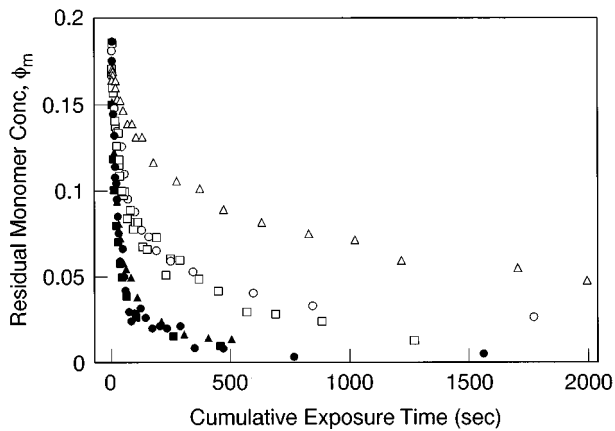


FIG. 11. Concentration of monomer  $\phi_m$  remaining as a function of cumulative exposure time for interrupted exposure using small-step exposure increments for the NVC system. The exposure intensities in  $\text{mW}/\text{cm}^2$  are 1.3 ( $\Delta$ ), 6.0 ( $\circ$ ), 7.8 ( $\square$ ), 40 ( $\blacktriangle$ ), 72 ( $\blacksquare$ ), and 93 ( $\bullet$ ). The monomer concentration was measured by NIR spectroscopy.

### B. Cure-dependent reaction rate

Next, we consider the photosensitivity of the NVC system. The concentration of monomer as a function of cumulative exposure time in the experiments with small, interrupted doses is plotted for each exposure intensity in Fig. 11. In Fig. 12, these data are replotted as a function of total exposure dose, that is, the exposure time multiplied by the exposure intensity. Note that for all but the highest intensity, 93  $\text{mW}/\text{cm}^2$ , the data superpose, indicating that the cure is a simple function of total dose for intensities ranging from 1.3 to 72  $\text{mW}/\text{cm}^2$ . However, the data for the highest exposure intensity, 93  $\text{mW}/\text{cm}^2$ , do not follow the same curve; at a given dose, there is a higher residual concentration of monomer (i.e., lower cure) for 93  $\text{mW}/\text{cm}^2$  than for the other intensities. Thus, the reaction rate seems to saturate when the exposure intensity exceeds a value around 70–80  $\text{mW}/\text{cm}^2$ . Hence, if one writes holograms with exposure intensities much in excess of this value one expects nonlinearities in the

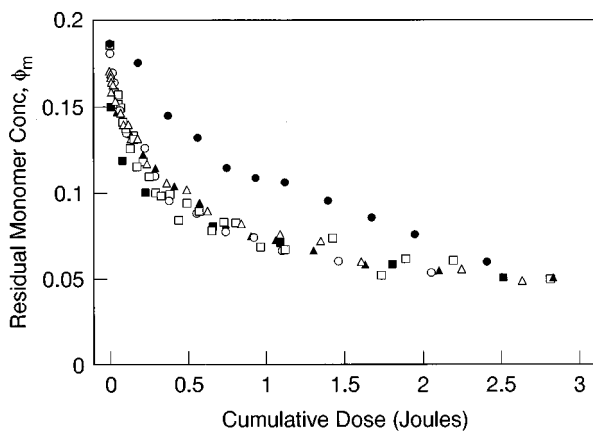


FIG. 12. Concentration of monomer  $\phi_m$  remaining as a function of cumulative exposure dose (exposure intensity times time) at the exposure intensities given in Fig. 11 for interrupted exposure with small-step exposure increments, for the NVC system. The symbols have the same meaning as in Fig. 11.

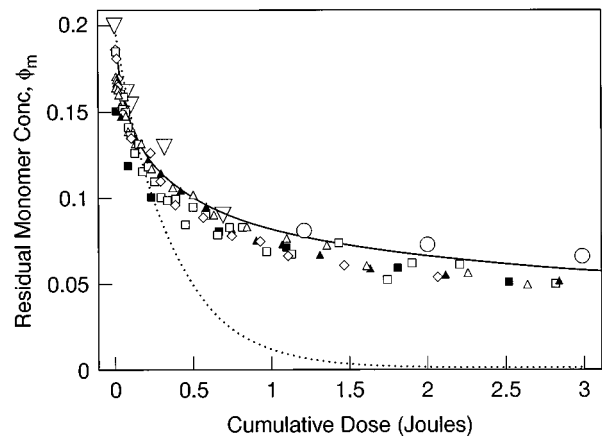


FIG. 13. All symbols are the same as in Fig. 12, except that large symbols are added for continuous exposures at an intensity of 2.25 ( $\nabla$ ) and 7.64  $\text{mW}/\text{cm}^2$  ( $\circ$ ). The dashed line is a “fit” to the data using an exponential decay obtained from a model with a reaction rate that is linear in remaining monomer concentration. The solid line is a fit using a diffusion-controlled reaction rate, Eq. (4), with  $R(0) = 0.3 \times 10^{-5} (\text{mW}/\text{cm}^2)^{-1} \text{s}^{-1}$ .

cure kinetics; a sinusoidal light intensity variation would produce a nonsinusoidal cure profile, with flattened maxima.

The dependence of the cure on total dose only at intensities less than 70  $\text{mW}/\text{cm}^2$  is contrary to the behavior expected from standard theories for free-radical reactions, which predict that the reaction rate is proportional to the square root of exposure intensity.<sup>14</sup> As discussed below, the reaction rate in this system appears to be controlled by the rate of diffusion, rather than the rate of reaction, and thus standard free-radical reaction kinetics do not seem to be appropriate for this system. This is fortuitous, since a square-root dependence of reaction rate on light exposure would introduce additional nonlinearities into the process of hologram formation.

Figure 13 tests the effect of the exposure history on the degree of cure. Each large filled symbol in Fig. 13 represents a run in which the starting sample had the same initial degree of precure,  $\phi_m \approx 0.20$ , but the sample was exposed continuously for time increments that varied from 30 to 400 s at exposure intensities of either 2.25 or 7.64  $\text{mW}/\text{cm}^2$ . The results for continuous exposure are in reasonably good agreement with those for interrupted exposure with  $I \leq 70 \text{ mW}/\text{cm}^2$ , although the reaction rate appears to be a bit slower for continuous exposure than it is for interrupted exposure. This could be due to exothermic heating, which tends to impede the reaction, or, more likely, the result of the dark reactions, which occur when the sample is not exposed. Nevertheless, to a good approximation, the degree of cure is controlled by the cumulative exposure, and not by its time history or the light intensity, as long as the intensity is less than around 70  $\text{mW}/\text{cm}^2$ .

The dashed line in Fig. 13 is a “fit” of an exponential decay to the initial portion of the kinetics data. The very poor fit shows that the reaction rate is highly nonlinear in monomer concentration, and slows down at low monomer concentration to an extent greater than that predicted by Eq. (1) with  $F$  constant. The slow down is consistent with a diffusion-controlled reaction rate, with the diffusion constant decreasing

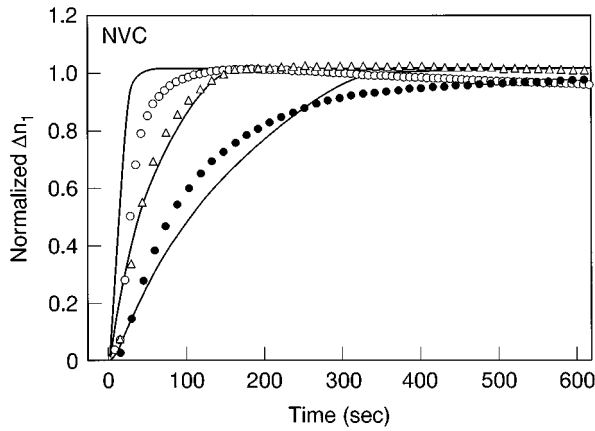


FIG. 14. Growth of normalized  $\Delta n_1$  in NVC at an exposure of  $2.25 \text{ mW/cm}^2$  and  $d=852 \text{ nm}$  at exposure times of 23 ( $\circ$ ), 135 ( $\triangle$ ), and 300 ( $\bullet$ ) s, and initial cure levels of 83.2%, 81.2%, and 86.7%, respectively. The symbols are the measured results and the lines are the predictions, using Eqs. (1), (3), and (4), and the values of  $D(0)=3.57 \times 10^{-14} \text{ cm}^2/\text{s}$  and  $R(0)=0.3 \times 10^{-5} (\text{mW/cm}^2)^{-1} \text{ s}^{-1}$ .

ing at lower monomer concentration (higher cure). As suggested in Sec. II, the rate coefficient  $F$  should be proportional to the diffusion constant, with proportionality constant  $R(0)$ , see Eq. (4). A value of  $R(0)=0.3 \times 10^{-5} (\text{mW/cm}^2)^{-1} \text{ s}^{-1}$  gives a good fit to the cure data for NVC as shown by the solid line in Fig. 13. The quality of the match between the solid line and the data in Fig. 13 adds support to the supposition of a diffusion-limited reaction rate, at least for the high precure levels examined here ( $<0.80$ ).

## V. MODELING HOLOGRAM STRENGTH AND NONLINEARITIES

Having developed model expressions for both the diffusivity and reaction rate, we can now predict the growth of  $\Delta n_1$  when ‘‘high’’ intensity gratings are written, in which both the diffusivity  $D$  and the reaction rate vary significantly both spatially and in time during the writing process. If we have modeled correctly the diffusion and reaction processes, it should be possible to predict the growth of  $\Delta n_1$  by solving Eq. (1) using Eqs. (3) for the diffusivity and (4) for the reaction rate  $F$ , with coefficients  $D(0)$  and  $R(0)$  as determined in Sec. IV. Figure 14 shows that the experimental growth curves of normalized  $\Delta n_1$  for exposure times of 23, 135, and 300 s at an exposure intensity of  $2.25 \text{ mW/cm}^2$  in NVC indeed agree well with the predicted curves. This agreement provides strong evidence for the basic validity of the diffusion model. Since  $D(\phi_m)$  and  $F(\phi_m)$  have the same dependences on  $\phi_m$  [see Eqs. (3) and (4)], the dimensionless ratio  $F(\phi_m)/D(\phi_m)k^2$  is a constant throughout the cure, and for Fig. 14 has the value 0.04.

In the above, predicted and measured values of  $\Delta n_1$  were compared on a normalized basis only. To predict the magnitudes of  $\Delta n_1$  and higher harmonics, a value must be assigned to the index-of-refraction contrast  $\Delta n \equiv n^d - n^h$ . The harmonics of the index-of-refraction profile comprising the hologram can then be obtained by simple multiplication:

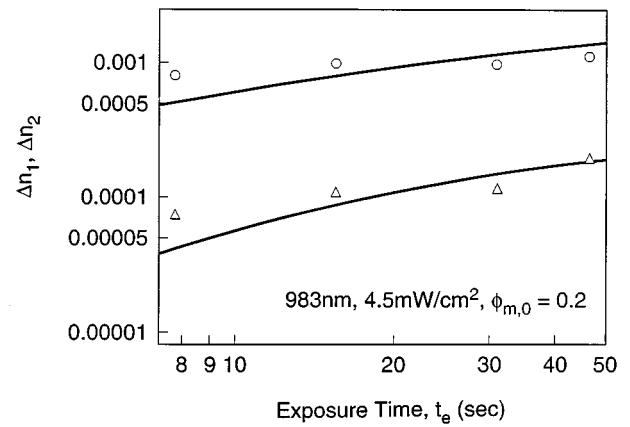


FIG. 15. Measured (symbols) and predicted (lines) values of the first and second harmonics  $\Delta n_1$  ( $\circ$ ) and  $\Delta n_2$  ( $\triangle$ ) of the index of refraction for NVC at an exposure intensity of  $4.5 \text{ mW/cm}^2$ , grating spacing of  $983 \text{ nm}$ , and initial monomer concentration of  $0.20$ . The lines are the predictions of the model with the index-of-refraction contrast  $\Delta n$  adjusted to  $0.025$  to obtain a best fit.

$$\Delta n_1 = \Delta n \Delta \phi_1; \quad \Delta n_2 = \Delta n \Delta \phi_2; \quad \Delta n_3 = \Delta n \Delta \phi_3. \quad (10)$$

Since the magnitude  $\Delta n$  of the contrast in index of refraction between the diffusant and the host materials is the small difference of much larger quantities ( $\Delta n/n_d \approx 0.01-0.02$ ), it is hard to obtain  $\Delta n$  with sufficient accuracy for meaningful tests of the model. We shall therefore obtain  $\Delta n$  by fitting the model to  $\Delta n_1$  and  $\Delta n_2$  measurements at one set of writing conditions. Figure 15 shows the measured and predicted first and second harmonics of the final hologram (after cessation of diffusion) as a functions of the exposure time for a  $983 \text{ nm}$  gratings written in NVC at an exposure intensity of  $4.5 \text{ mW/cm}^2$ . Under these conditions, the sample is rather underexposed ( $F(\phi_m)/D(\phi_m)k^2=0.09$ ), and  $\Delta n_2$  is much less than  $\Delta n_1$ . The predictions of the model fit the data well, with a best-fit value of  $\Delta n$  of  $0.025$ . Note that the model accurately predicts that ratio  $\Delta n_2/\Delta n_1$  is around  $0.1$  under these conditions.

Having obtained  $\Delta n$  by this successful fit in Fig. 15, comparisons between the model predictions and experimental data at other writing conditions can then be made without adjustable parameters. Figure 16 shows measurements of  $\Delta n_1$ ,  $\Delta n_2$ , and  $\Delta n_3$  as a function of writing time under stronger exposure conditions, that is, for  $1540 \text{ nm}$  gratings and an exposure intensity of  $30 \text{ mW/cm}^2$ , so that  $F(\phi_m)/D(\phi_m)k^2=1.5$ . The wider grating slows down the diffusion and the higher light intensity speeds up the reaction, so that the second and third harmonics become larger relative to the first harmonic as the exposure time increases. This trend, and indeed the magnitudes of all three harmonics are accurately predicted by the model, with no adjustable parameters. The major discrepancy between the predictions and the measurements in Fig. 16 occurs at long exposure times, where the measured second and third harmonics fall modestly below the predicted values.

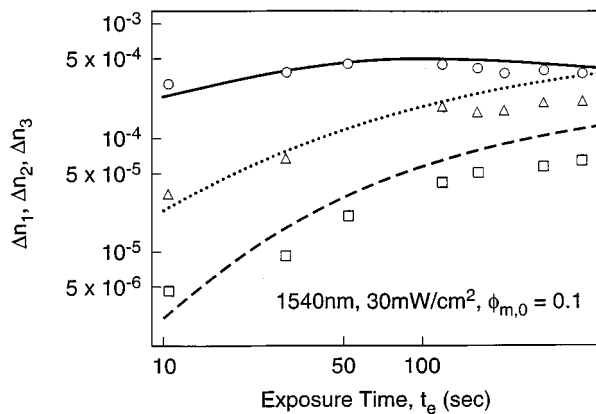


FIG. 16. Measured and predicted values of the first ( $\circ$ ), second ( $\Delta$ ), and third ( $\square$ ) harmonic of the index of refraction for NVC at an exposure intensity of  $30 \text{ mW/cm}^2$ , a grating spacing of  $1540 \text{ nm}$ , and an initial monomer concentration of  $0.10$ .

## VI. SUMMARY

This modeling study shows that the process of grating formation in photosensitive polymers can readily be interpreted in terms of diffusion of monomer into zones in which it has been partially converted to polymer due to high light intensities. The strength of the resulting diffraction pattern is controlled by the magnitude of the concentration differences created by this diffusion, and by the contrast in the index of refraction between the diffusant and the host matrix in which it moves. The time scale for formation of the grating is determined by the diffusion coefficient of the monomer and by the width of the grating spacing.

Quantitative prediction of the growth rate of the grating is complicated by the dependencies of both the reaction rate and the diffusivity on the monomer concentration. However, these dependencies can be measured by near-infrared data and by the rate of hologram buildup after writing small gratings. The cure-dependent diffusion coefficient for the acry-

late system studied here can be fit by a simple free-volume theory. The reaction rate coefficient proves to be simply proportional to the diffusivity. This, along with the observation that the reaction rate coefficient depends linearly on light intensity over a wide range of exposure intensities, suggests that the reaction is diffusion controlled, and allows the reaction kinetics to be accounted for by a single-parameter expression, once the cure dependence of the diffusion coefficient is known.

Thus, the nonlinearities in the diffusion and reaction rates can readily be measured and accounted for. Accurate predictions can then be made of the rate of hologram formation under nonlinear writing conditions, and the magnitudes of the first, second, and third harmonics of the index of refraction can be accurately predicted. Thus, the model can aid in optimizing the performance of a given material, and help guide the design of materials with superior performance. The model should also be capable of describing other systems, such as that of DuPont, if the relevant kinetic and diffusion data are measured.

- <sup>1</sup>W. S. Colburn and K. A. Haines, *Appl. Opt.* **10**, 1636 (1971).
- <sup>2</sup>R. H. Wopschall and Pampalone, *Appl. Opt.* **11**, 2096 (1972).
- <sup>3</sup>B. L. Booth, *Appl. Opt.* **14**, 593 (1975).
- <sup>4</sup>W. J. Tomlinson and E. A. Chandross, *Adv. Photochem.* **12**, 201 (1980).
- <sup>5</sup>W. K. Smothers, B. M. Monroe, A. M. Weber, and D. E. Keys, *Proc. SPIE* **1212**, 20 (1990).
- <sup>6</sup>U.-S. Rhee, H. J. Caulfield, C. S. Vikram, and J. Shamir, *Appl. Opt.* **34**, 846 (1995).
- <sup>7</sup>J. D. Ferry, *Viscoelastic Properties of Polymers*, 3rd ed. (Wiley, New York, 1980).
- <sup>8</sup>G. Zhao and P. Mouroulis, **115**, 528 (1995).
- <sup>9</sup>*Processes in Photoreactive Photopolymers*, edited by V. Krongauz and A. D. Trifunac (Chapman & Hall, New York, 1995), pp. 316–318.
- <sup>10</sup>G. Zhao and P. Mouroulis, *J. Mod. Opt.* **41**, 1929 (1994).
- <sup>11</sup>H. Fujita and A. Kishimoto, *J. Chem. Phys.* **34**, 393 (1961).
- <sup>12</sup>J. Xia and C. H. Wang, *J. Polym. Sci. Polym. Phys. Ed.* **33**, 899 (1995).
- <sup>13</sup>H. K. Kogelnik, *Bell Syst. Tech. J.* **48**, 2909 (1969).
- <sup>14</sup>F. W. Billmeyer, *Textbook of Polymer Science* (Wiley, New York, 1971), p. 290, Eqs. (9) and (10).